

AD-A031 556

NAVAL RESEARCH LAB WASHINGTON D C
REALIZATION OF A RELATIVISTIC MIRROR: ELECTROMAGNETIC BACKSCATT--ETC(U)
SEP 76 V L GRANATSTEIN, P SPRANGLE
NRL-MR-3373

F/G 20/3

UNCLASSIFIED

NL

[OF]

AD
A031556



END

DATE

FILMED

12-76

FL (12)
NRL Memorandum Report 3373

Realization of a Relativistic Mirror: Electromagnetic Backscattering from the Front of a Magnetized Relativistic Electron Beam

V. L. GRANATSTEIN, P. SPRANGLE, R. K. PARKER,
J. PASOUR, M. HERNDON, AND S. P. SCHLESINGER

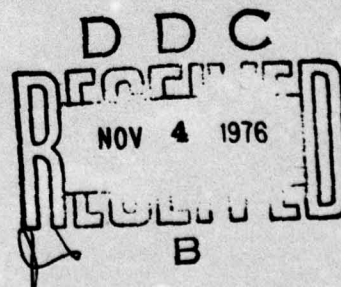
Plasma Physics Division

and

J. L. SEFTOR

*Science Applications Incorporated
McLean, Virginia 22101*

September 1976



NAVAL RESEARCH LABORATORY
Washington, D.C.

ADA031556

SECURITY CLASSIFICATION OF THIS PAGE (When Data Entered)

REPORT DOCUMENTATION PAGE		READ INSTRUCTIONS BEFORE COMPLETING FORM
1. REPORT NUMBER NRL Memorandum Report 3373	2. GOVT ACCESSION NO. 14 NRL-MR-3373	3. RECIPIENT'S CATALOG NUMBER
4. TITLE (and Subtitle) 6 REALIZATION OF A RELATIVISTIC MIRROR: ELECTROMAGNETIC BACKSCATTERING FROM THE FRONT OF A MAGNETIZED RELATIVISTIC ELECTRON BEAM	5. TYPE OF REPORT & PERIOD COVERED 9 Interim report on a continuing NRL problem	6. PERFORMING ORG. REPORT NUMBER
7. AUTHOR(s) 10 V.L. Granatstein, P. Sprangle, R.K. Parker, J. Pasour, M. Herndon, S.P. Schlesinger†, and J.L. Seftor‡	8. CONTRACT OR GRANT NUMBER(s)	
9. PERFORMING ORGANIZATION NAME AND ADDRESS Naval Research Laboratory Washington, D.C. 20375	10. PROGRAM ELEMENT, PROJECT, TASK AREA & WORK UNIT NUMBERS NRL Problem R08-59 Subtask RR0110941	
11. CONTROLLING OFFICE NAME AND ADDRESS 12 33 p.	12. REPORT DATE 11 September 1976	13. NUMBER OF PAGES 32
14. MONITORING AGENCY NAME & ADDRESS (if different from Controlling Office)	15. SECURITY CLASS. (of this report) UNCLASSIFIED	15a. DECLASSIFICATION/DOWNGRADING SCHEDULE
16. DISTRIBUTION STATEMENT (of this Report) Approved for public release; distribution unlimited.		
17. DISTRIBUTION STATEMENT (of the abstract entered in Block 20, if different from Report)		
18. SUPPLEMENTARY NOTES *Present address: Department of Physics, North Carolina State University, Raleigh, North Carolina. †Also of Department of Electrical Engineering and Computer Science, Columbia University, New York, New York 10025. ‡Science Applications Incorporated, McLean, Virginia 22101.		
19. KEY WORDS (Continue on reverse side if necessary and identify by block number) Microwaves Electron beam Electromagnetic Radiation <i>f sub i f sub a Paul i</i>		
20. ABSTRACT (Continue on reverse side if necessary and identify by block number) An intense relativistic electron beam has been injected into a cylindrical drift tube containing a counterstreaming electromagnetic wave ($f_i = 9.3$ GHz and $P_i = 170$ kW). Within a narrow range of axial magnetic field centered at 5 kG, a reflected wave at $f_s \sim 40$ GHz was generated by the interaction of the beam with the incident wave. The reflected wave was observed to have a power of several hundred kilowatts (i.e. greater than the power of the incident wave) and a pulse duration on the order of nanoseconds. All observed experimental characteristics (viz. frequency shift, power <i>approximately</i> (Continues) <i>next page</i>		

DD FORM 1 JAN 73 1473

EDITION OF 1 NOV 65 IS OBSOLETE
S/N 0102-014-6601

1


251 950

SECURITY CLASSIFICATION OF THIS PAGE (When Data Entered)

mt

20. Abstract (Continued)

amplification, pulse duration, and cyclotron resonance) were consistent with a model of reflection from the discontinuity in refractive index that is associated with an electron beam front near cyclotron resonance. This mechanism could be employed in a new class of short-pulse, ultra-high power, tunable generators at millimeter and submillimeter wavelengths.



CONTENTS

I. INTRODUCTION	1
II. BEAM FRONT SCATTERING IN FINITE GEOMETRY	2
III. EXPERIMENTAL	6
IV. DISCUSSION	8
V. CONCLUSIONS	11
VI. ACKNOWLEDGEMENTS	12
APPENDIX	23

ACCESSION for	
NTIS	Write Section <input checked="" type="checkbox"/>
DOC	Ref. Section <input type="checkbox"/>
UNANNOUNCED	<input type="checkbox"/>
JUSTIFICATION	
BY	
DISTRIBUTION/AVAILABILITY CODES	
Dist.	AVAIL. and/or SPECIAL
A	

**REALIZATION OF A RELATIVISTIC MIRROR:
ELECTROMAGNETIC BACKSCATTERING FROM THE FRONT
OF A MAGNETIZED RELATIVISTIC ELECTRON BEAM**

I. INTRODUCTION

A reflector of electromagnetic energy which moved at relativistic speed (relativistic mirror) would have intriguing properties. A back-scattered wave would have a much larger frequency than the incident wave because of the Doppler effect. In addition, if the scattering were efficient, energy amplification would be realized. Recent studies have shown that a relativistic electron beam may well be the most practical embodiment of such a relativistic mirror. A number of analyses¹⁻⁵ pertinent to stimulated scattering from density waves in the body of relativistic electron beams have appeared, and the first experimental observations of stimulated scattering have been reported.^{6,7}

In this paper, we describe an observation which admits of a simpler interpretation: an incident electromagnetic wave has apparently been reflected off the refractive index discontinuity at the front of a magnetized, relativistic electron beam. The utilization of such scattering was first suggested by Landecker.⁸ He considered the case of a plane wave (frequency ω_i , total energy W_i , Poynting flux p_i) incident on a semi-infinite beam characterized by its average speed \bar{v} and the corresponding relativistic parameters $\beta = \bar{v}/c$ and $\gamma = (1 - \beta^2)^{-1/2}$. He showed that the backscattered wave would be characterized by a frequency

$$\omega_s = (1 + \beta)^2 \gamma^2 \omega_i, \quad (1)$$

corresponding to a total scattered energy

$$W_s = (1 + \beta)^2 \gamma^2 W_i, \quad (2)$$

Note: Manuscript submitted September 3, 1976.

where R is the coefficient of reflection of the beam front in the beam frame. These relationships also characterize the stimulated scattering process mentioned above. However, unlike stimulated scattering from the body of the electron beam, beam front scattering is characterized by a time compression of the scattered wave. With this compression, the scattered Poynting flux is enhanced by a greater factor than the scattered energy, viz.

$$p_s = (1 + \beta)^4 \gamma^4 R p_i . \quad (3)$$

In the present work, we have scattered an incident wave at $\lambda = 3.2$ cm from the front of a relativistic electron beam to produce a scattered wave at $\lambda \approx 8$ mm. The frequency conversion factor agrees well with that given in Eq. (1). Also some power amplification occurred with the power in the scattered 8 mm wave exceeding the power in the 3.2 cm incident wave. In Section II below we present an analysis of beam front scattering in a geometry modeling the experimental configuration. The experimental method and results are presented in Section III. Discussion and conclusions are in Sections IV and V respectively.

II. BEAM FRONT SCATTERING IN FINITE GEOMETRY

In order to carry out a more realistic analysis, we have departed from the unbounded geometry analyzed by Landecker and instead have employed the model depicted in Fig. 1. In this figure, a solid cylindrical electron beam of radius r_b is traveling through a drift tube of radius r_g at a speed \bar{v} . Initially, the drift tube is filled with electromagnetic radiation generated by an external wave source. The frequency of this incident wave, ω_i , is chosen so that only the fundamental waveguide mode of the drift tube (TE_{11}) can propagate in the empty tube. The normalized group velocity of the injected wave in the empty tube is given by $\beta_g = c^{-1} \partial \omega_i / \partial k_{z1} = (1 - b_{11}^2 c^2 / \omega^2)^{1/2}$ where $b_{11} = 1.84 / r_g$.

In this bounded geometry Eqs. (1) (2) and (3) will be somewhat modified. The frequency of a backscattered wave will be given by

$$\omega_s = \gamma^2(1 + \beta^2 + 2\beta\beta_g)\omega_i, \quad (4)$$

while the energy of a backscattered wave W_s will be related to the incident wave energy W_i by

$$\frac{W_s}{W_i} = \frac{\omega_s}{\omega_i} RW_i = \gamma^2(1 + \beta^2 + 2\beta\beta_g)RW_i. \quad (5)$$

The time during which the incident wave source supplies energy that eventually interacts with the electron beam is given by

$$\tau_i = \frac{L}{c} \left(\frac{1}{\beta} + \frac{1}{\beta_g} \right), \quad (6)$$

where L is the length of the drift tube. The time, τ_i , consists of two parts: 1) $L/(c\beta_g)$, the time for the incident wave to fill the empty tube, and 2) $L/c\beta$, the time for the beam front to propagate through the tube. We assume that the source continues to supply field energy throughout the scattering process.

The time duration of the backscattered pulse is given by

$$\tau_s = \frac{L}{c} \left(\frac{1}{\beta} - \frac{1}{\beta_{gs}} \right), \quad (7)$$

where β_{gs} is the group velocity of the scattered wave, viz.

$$\beta_{gs} = \beta_g \left(1 + \beta^2 + 2\beta\beta_g^{-1} \right) / \left(1 + \beta^2 + 2\beta\beta_g \right).$$

Then, to relate the power in the scattered wave to the power in the incident wave, one may use Eqs. (5) - (8) as follows:

$$\frac{P_s}{P_i} = \frac{W_s}{W_i} \frac{\tau_i}{\tau_s} = \frac{\omega_s^2}{\omega_i^2} \frac{\beta_{gs}}{\beta_g} R = \gamma^4 (1 + \beta^2 + 2 \beta \beta_g) (1 + \beta^2 + 2 \beta \beta_g^{-1}) R. \quad (9)$$

Clearly, the conditions which favor large power amplification are: (1) highly energetic electrons ($\gamma \gg 1$, $\beta \rightarrow 1$); (2) an incident wave near cutoff ($\beta_g \rightarrow 0$); and, (3) a highly reflective beam front ($R \rightarrow 1$). Then, $P_s \sim 4 \gamma^4 \beta_g^{-1} P_i$ which will exceed Eq. (3) by β_g^{-1} .

It is now appropriate to consider under what conditions the electron beam will reflect the incident wave. Reflection will occur near the intersection of the waveguide dispersion curve

$$\frac{\omega^2}{c^2} - k_z^2 - b_{11}^2 = 0, \quad (10)$$

in the empty drift tube and the propagation line for the fast beam cyclotron mode

$$\frac{\omega}{c} - k_z \beta - \frac{\Omega_0}{c\gamma} = 0, \quad (11)$$

where $\Omega_0 = e\bar{B}/m_0$ is the electron cyclotron frequency.

It is shown in the appendix that the dispersion relation for the waveguide-electron beam system is of the form

$$\left(\frac{\omega^2}{c^2} - k_z^2 - b_{11}^2 \right) \left(\frac{\omega}{c} - k_z \beta - \frac{\Omega_0}{c\gamma} \right) = \omega_p^2 F(k_z, \omega), \quad (12)$$

where $\omega_p = \left(\frac{e^2 n}{\epsilon_0 m_0 \gamma} \right)^{1/2}$ is the invariant plasma frequency, n is the electron number density, and F is a complicated real function of wavenumber and frequency.

In general, Eq. (10) and (11) cannot be satisfied for real ω and real k_z unless the electron density vanishes. Rather, if one assumes a nonzero electron density, and specifies a value of ω to fall near the intersection of Eqs. (10) and (11), then the dispersion relation in Eq. (12) is satisfied only for complex k_z . This implies the appearance of a stop band in which the wave is reflected.

If we consider a one-dimensional, sharp, beam front, then there are two distinct regions for the incident wave; region I ahead of the beam front and region II within the magnetized beam (see Fig. 1). Assuming that the beam moves at a constant velocity, first choose the wave frequency such that the wave can propagate into region II. It is clear in that case that, in the beam frame, this frequency is continuous across regions I and II. The wavenumber in this frame, however, undergoes an abrupt change across the interface. Transforming this jump in wavenumber back to the laboratory frame implies that both the wavenumber and frequency of the wave experience an abrupt change across the beam-vacuum interface. This frequency jump is not necessarily associated with reflections but is due simply to the fact that a jump in the wavenumber in the beam frame, $\Delta k'$, appears as a frequency jump in the laboratory frame, $\Delta\omega = \gamma\bar{v}\Delta k'$. The typical dispersion characteristics in the laboratory frame shown in Fig. 2 illustrates these points. The solid curve represents the plot of $\text{Re}(\omega)$ vs $\text{Re}(k_z)$ in region II, while the dashed curve depicts the dispersion relation in region I. Now consider the wave in region I which corresponds to point a in the figure. This wave when it enters region II jumps to point a' (along a line with slope \bar{v}) and, thereby, undergoes a small decrease in frequency and a small increase in wavenumber. A wave at point b also propagates into the beam

but at a higher frequency and smaller wavenumber corresponding to point b' . The wave in region I at point c is in the stop band and cannot propagate into region II. Instead, it undergoes reflection at the beam front and goes to point c' still in region I. The frequency enhancement in going from c to c' is given by Eq. (4).

The prediction of 100% reflection for a wave appropriately placed in the stop band is a consequence of the 'sharp' beam front assumption in the simple theory above. In practice, the beam front region will be characterized by finite gradients in both electron density and electron energy, and the reflectivity will be substantially less than 100%.

III. EXPERIMENTAL

The intense relativistic electron beam used in the beam front scattering experiments was generated by applying a voltage pulse of maximum value $V_0 = 900$ kV from a moderate-impedance, pulse-forming-line⁹ to a foilless, field-emission diode.¹⁰ The electron beam was injected through the diode region into an evacuated axially magnetized drift tube.

The voltage pulse waveform applied to the cathode is shown in Fig. 3 together with the drifting current pulse waveform measured by means of a Faraday cup. The voltage pulse has a risetime of 13 nsec while the current risetime is 9 nsec. Following the initial rise, each pulse amplitude remained relatively constant for a duration of ~ 50 nsec. During this interval, the drift tube current is ~ 2 kA indicating a beam impedance in the plateau region of ~ 450 ohms. The radial current profile was estimated by placing a Lucite witness plate within the drift tube. The damage pattern formed on the plate is shown in Fig. 4 as an annulus with o.d. ~ 11 mm and thickness ~ 2 mm.

After these preliminary beam measurements, the experimental configuration shown in Fig. 5 was used to introduce into the drift tube a microwave signal propagating counter to the electron beam. This wave source was a magnetron which supplied an $\sim 0.5 \mu\text{sec}$ long pulse of 9.3 GHz radiation at a power level of 170 kW. This signal propagated in the electron drift tube in the fundamental TE_{11} mode with normalized group velocity $\beta_g = .514$. The presence of high frequency electromagnetic waves, resulting from the interaction of the electron beam with the injected microwaves, was indicated by a signal from a pyroelectric detector.

The high-frequency output line leading to the pyroelectric detector was separated from the drift tube by a periodically perforated plate with a hole radius $r_0 = 1 \text{ mm}$ and a periodicity $a = 3 \text{ mm}$. This plate acts as a gradual high-pass filter having a transmissivity¹¹

$$T = 4(4 + B^2)^{-1}, \quad (14)$$

where $B = (3/8\pi)(a/r_0)^3(\lambda/a)$.

The output signal, after passing the perforated plate, propagated through a length of gold-plated tubing with an inner diameter equal to 12 mm. This tubing effectively cut off all signals with $f < 14 \text{ GHz}$, ensuring that the 9.3 GHz signal did not reach the pyroelectric detector.

In Fig. 6, typical oscilloscope traces are displayed which demonstrate that the detection of a high frequency output signal was correlated with the simultaneous firing of the electron beam and the injected wave. The top traces are superpositions of the $0.5 \mu\text{sec}$ incident wave pulse and the voltage pulse applied to the diode of the electron accelerator (seen at this sweep speed as a sharp spike). The traces at the bottom show the high-frequency output on the pyroelectric detector. For the traces on the left-hand side, the

injected wave and the diode voltage pulse were not synchronized, and there was no high-frequency electromagnetic output. In the traces on the right-hand side, this incident wave was synchronized with the electron beam, and a strong high frequency output signal was observed.

Note that the time duration of the high-frequency output pulse was very short, much shorter than the 50 nsec duration of the electron beam. In fact, the recorded pulse time was so short that it probably was limited by the response time of the pyroelectric detector (viz; 5 nsec risetime); the actual signal pulse may therefore be even shorter than indicated in Fig. 6.

The wavelength of the high-frequency output wave was determined by using a number of mesh filters both in transmission and reflection. In Fig. 7, the measured normalized signal strengths with a filter placed in the output line are plotted against the filter mesh constant. Drawn on the same figure are the theoretical response curves for various wavelengths which were deduced from calibration data supplied by the manufacturer of the mesh filters (viz. Advanced Kinetics Inc.). A mean square error analysis indicated that the experimental data best fits the calibration curves for $\lambda = 8 \text{ mm}$ ($f = 37.5 \text{ GHz}$).

Lastly, the high frequency output power is shown as a function of magnetic field strength in Fig. 8. The plot shows a resonance in output power for magnetic field strengths between 4 kG and 6 kG.

IV. DISCUSSION

According to Eq. (4), an output frequency of $\sim 40 \text{ GHz}$ resulting from reflection of a pump wave at $\omega_1/2\pi = 9.3 \text{ GHz}$ and $\beta_g = .51$ indicates reflection from an ensemble of electrons with $\gamma \approx 1.3$ and $\beta \approx 0.6$. This implies that the active portion of the electron beam was in the beam front and

consisted of electrons which had been accelerated on the rising portion of the voltage pulse to a kinetic energy of ~ 150 keV.

Since the accelerating voltage has a finite risetime, the kinetic energy of the leading electrons at the beam front will vary as the front propagates along the drift tube. The slower electrons emitted early in the rise of the accelerating voltage will be progressively overtaken by the faster electrons emitted as the voltage continues to increase. If the total energy of the electrons entering the drift tube during the rise of the voltage pulse can be approximated by $\gamma = 1 + (eV_0/m_0 c^2)(t/t_R)$ the speed of the leading beam front electrons will vary with axial position as shown in Fig. 9. When $t_R = 10$ nsec, the leading beam front electrons have $\beta \approx 0.6$ over most of the drift tube. This is consistent with both the risetime of the voltage pulse as shown in Fig. 3 and the measured Doppler shift (Eq. 4).

The change in kinetic energy of the leading electrons as the beam front propagates through the drift tube implies that beam front scattering may take place only in certain parts of the tube. In Fig. 10, we have sketched some possible dispersion curves for waves propagating through the beam front (denoted by the solid lines). In Fig. 10a, near the cathode, the value of energy for the leading electrons (denoted by γ_1) is relatively small. The stop band for propagation through the beam front falls above the injected wave frequency ω_i , and no reflection occurs. Instead, this wave continues to propagate past the leading electrons into the part of the drift tube containing the electron beam. In Fig. 10b, the situation when the beam front has propagated further downstream is depicted. The value of γ for the leading electrons has increased to γ_2 ; the incident wave frequency now falls in the stop band; and, there is wave reflection off

the beam front. (Local homogeneity in the beam front region has been assumed to hold.)

The hypothesis of beam front scattering is supported by the short output pulse. According to Eq. (7), with a scattering region of length $L \approx 1$ m, the output pulse length would be $\tau_s \approx 2$ nsec. This is consistent with the output pulse length seen in Fig. 6. If scattering had been from density waves in the body of the beam rather than from the beam front, one would expect the output pulse length to be equal to the length of the electron current pulse (viz. ~ 50 nsec).

The range of magnetic field over which the high frequency signal was observed (see Fig. 8) is also consistent with a picture of beam front scattering. In Fig. 11 the dispersion curve is plotted for the TE_{11} mode in the presence of a magnetized electron beam partially filling a drift tube of 22 mm diameter. The beam parameters were chosen to approximate those in the active part of the beam front (viz. $\gamma = 1.3$, beam diameter = 11 mm, and $I \approx 150$ kV/450 ohms = 330 A which corresponds to $\omega_p/2\pi = 3$ GHz). The magnetic field strength was chosen as 5.7 kG which falls within the resonance region shown in Fig. 8. As seen in Fig. 11, this choice of parameters places the injected wave frequency ($\omega_i/2\pi = 9.3$ GHz) near the intersection of the cyclotron beam line (Eq. 11) and the TE_{11} dispersion curve in the empty waveguide (Eq. 10).

Lastly, it is of interest to estimate the power in the scattered wave and compare it with the incident microwave power of 170 kW to determine if power amplification occurred. The scattered power entering the pyroelectric detector at resonance was 7 kW corresponding to the maximum value in Fig. 8.

However, the scattered power in the drift tube is much larger than the detected power. The scattered wave is only partly transmitted by the perforated plate at the end of the drift tube (see Eq. (14)), and furthermore, the output line is smaller in diameter than the drift tube. When these factors are taken into account, the scattered power in the drift tube was estimated to have been ~ 300 kW, about twice as large as the incident wave power. This would correspond to a value of reflection coefficient $R \sim 6\%$.

To compare this value of power enhancement with theory requires a calculation of the reflectivity of the beam front. Such a calculation which considers the gradients in both electron density and electron energy is underway, and will be described in future publications. Preliminary results indicate that the effect of the gradients is to introduce absorption of the pump wave energy in addition to reflection. However, consideration of the development of the beam front gradients as the front propagates through the drift tube indicates that there will be a region of the drift tube in which strong reflection can still occur.

V. CONCLUSIONS

A microwave signal at 9.3 GHz has been scattered from an intense relativistic electron beam to produce an output electromagnetic wave at ~ 38 GHz. The frequency of the scattered wave, the pulse duration of the scattered signal, the values of magnetic field where the scattering was maximized, and the risetime of the voltage pulse used to accelerate the electrons are all consistent with a picture of scattering from an ensemble of electrons in the electron beam front. It also appears that power enhancement occurred with the power in the 38 GHz scattered wave being about twice as large as the pump wave power at 9.3 GHz.

The combined features of substantial frequency multiplication and power enhancement suggests that beam front scattering might well be an attractive process for the production of high power pulses at millimeter and submillimeter wavelengths. Unlike stimulated scattering, beam front scattering has the additional advantage of not requiring a threshold value of pump power, and may therefore be observed with moderate-power incident wave sources.

Furthermore, the output frequency should be readily tunable. The output frequency is of course controllable by varying the incident wave frequency. But beyond this, it should be possible to obtain a larger frequency multiplication by sharpening the rise in the voltage and current pulses. An experimental investigation of this effect is in progress.

VI. ACKNOWLEDGEMENTS

The authors thank J. L. Hirshfield and H. Fleischmann for their useful suggestions during the course of this work.

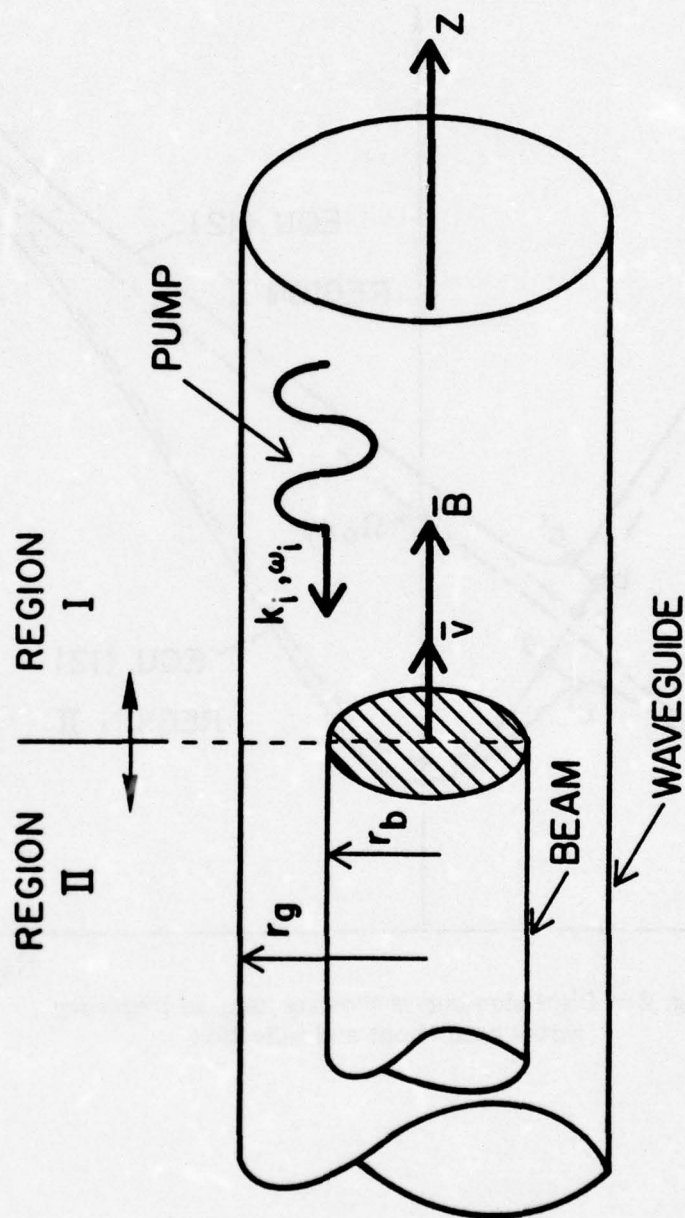


Fig. 1 — Model geometry for analysis of beam front scattering

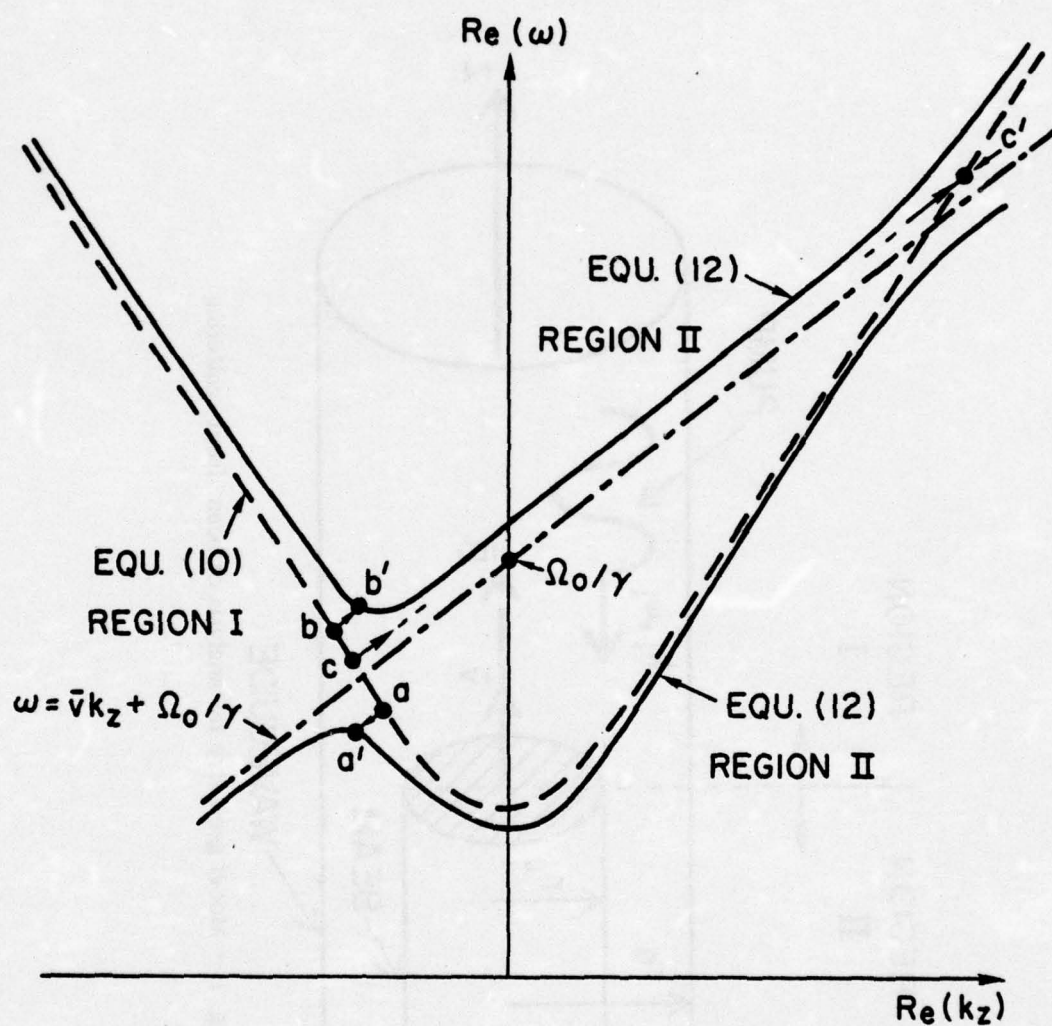


Fig. 2 — Dispersion curves showing jump in frequency across beam front and reflection

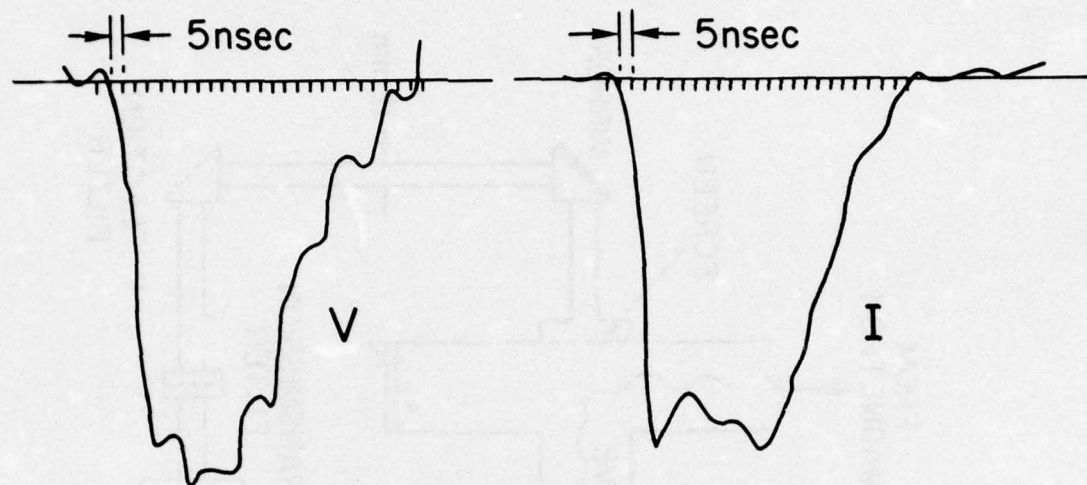


Fig. 3 — Diode voltage pulse and corresponding electron current pulse



Fig. 4 — Witness plate indicating radial profile of electron beam.
(Diameter of plate is 22 mm.)

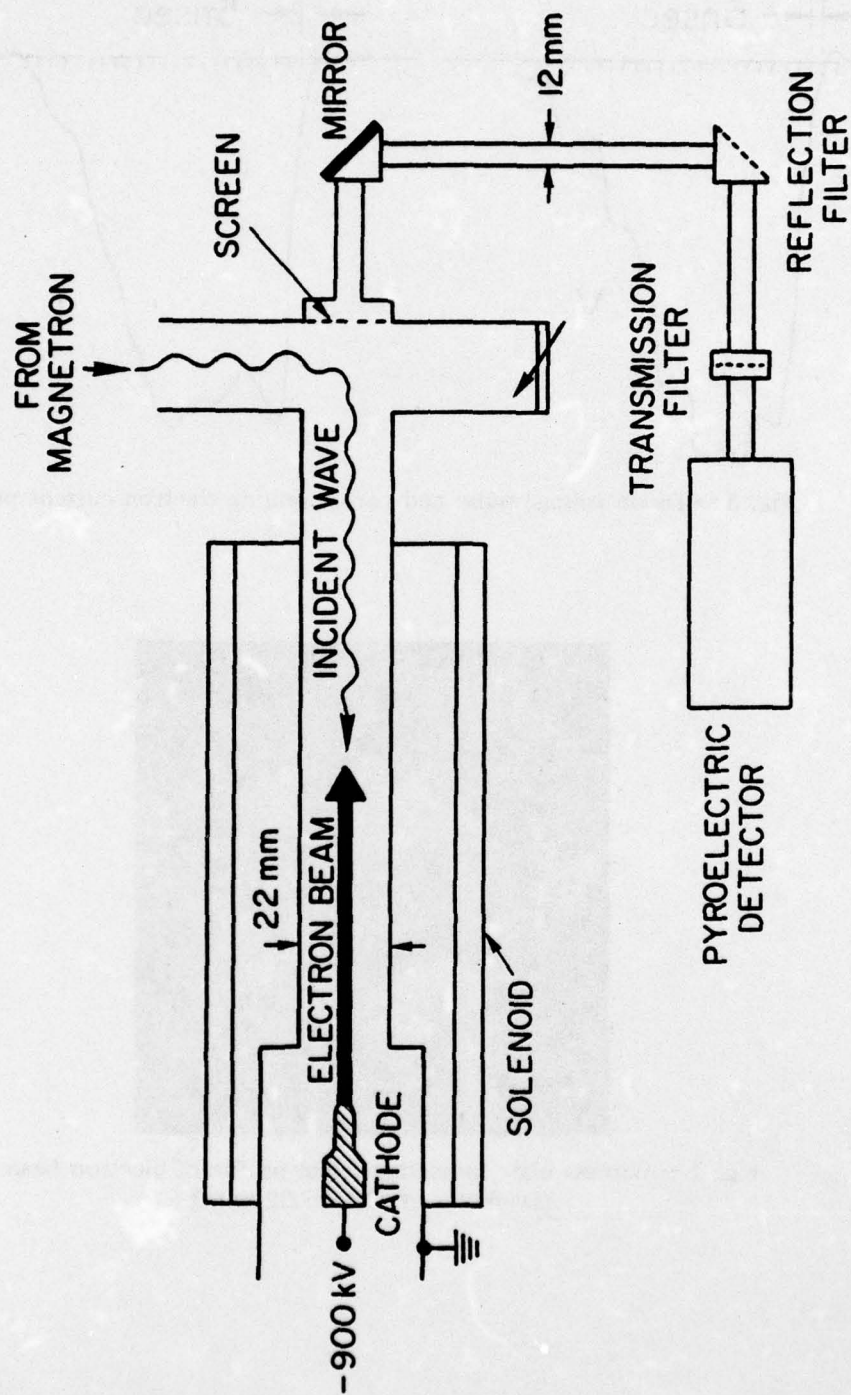


Fig. 5 — Experimental configuration

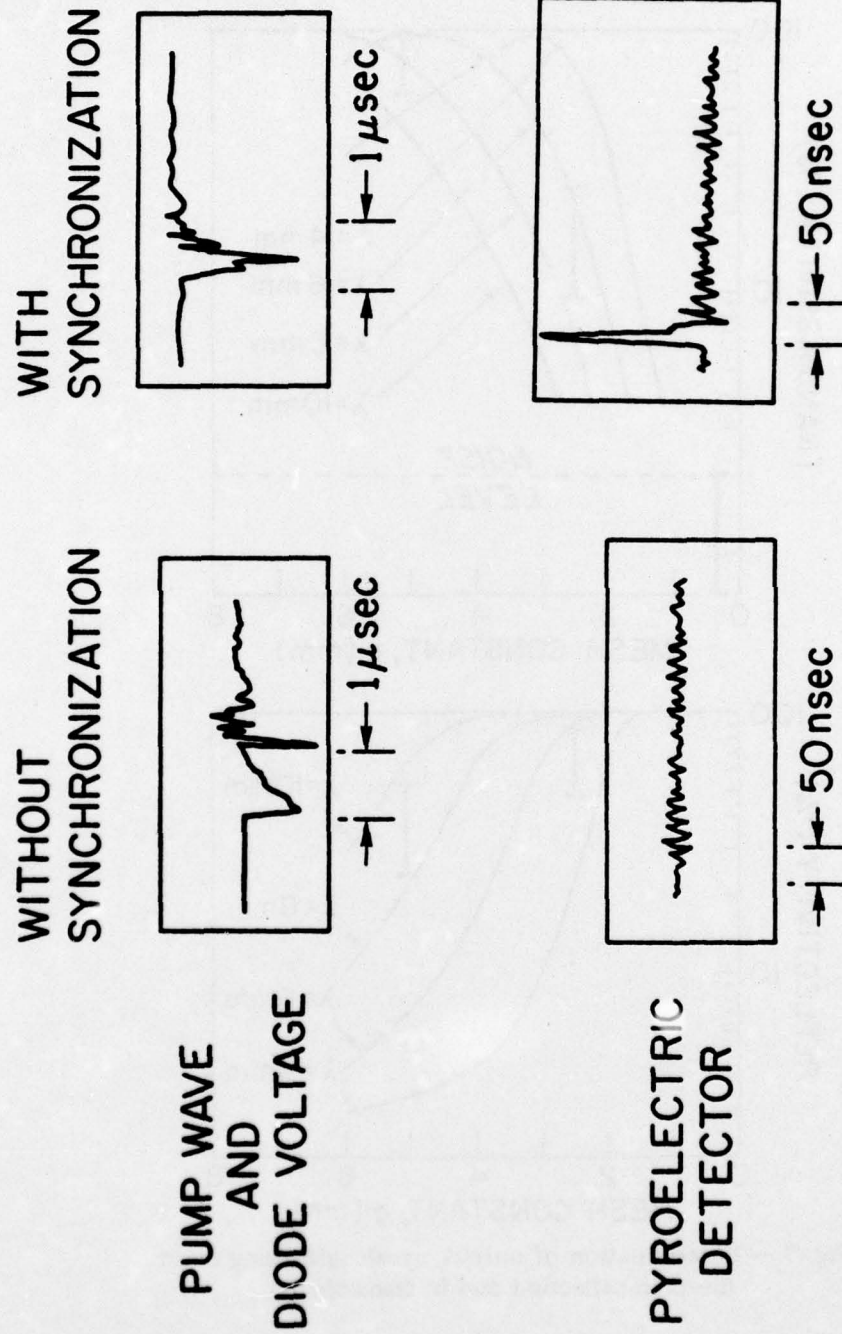


Fig. 6 — Oscilloscope traces showing that occurrence of high frequency output signal is correlated with simultaneous propagation of pump wave and electron beam through the drift tube

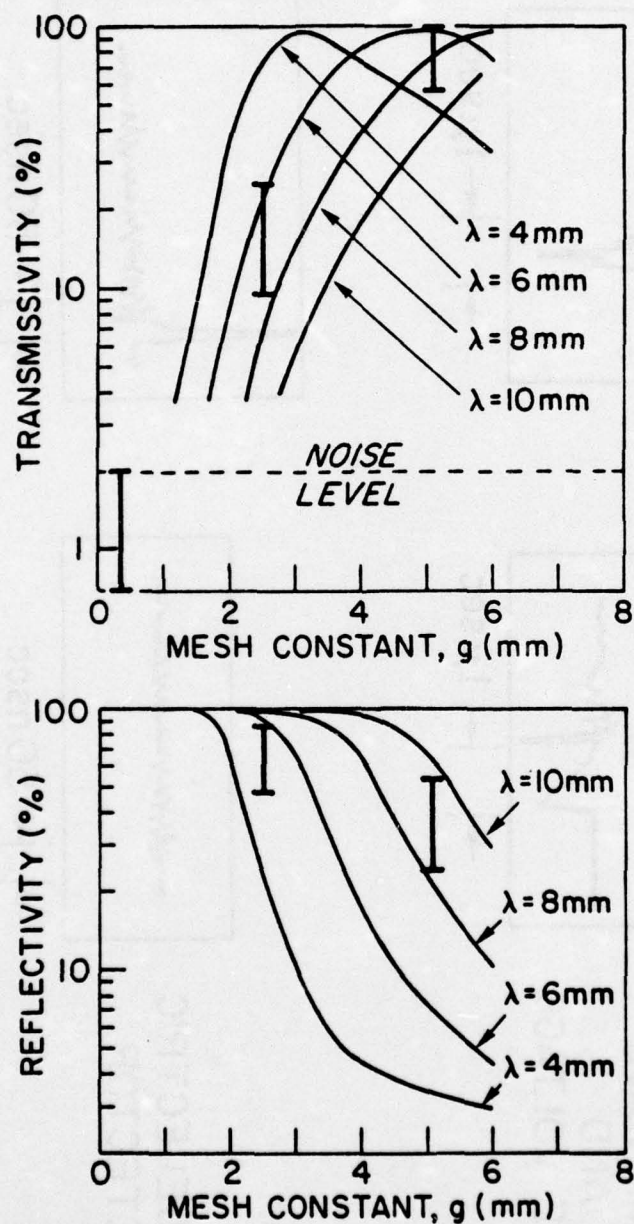


Fig. 7 — Determination of output wavelength using mesh filters in reflection and in transmission

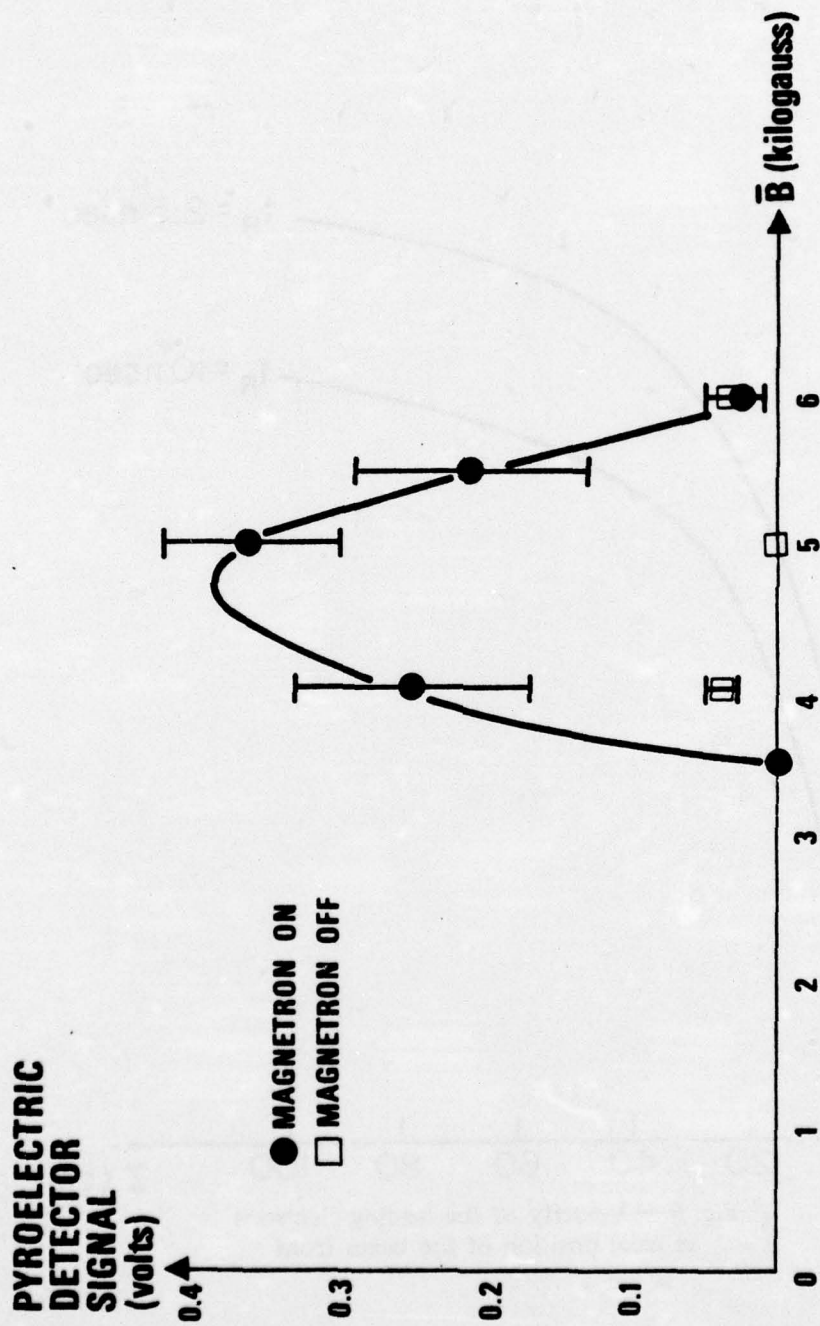


Fig. 8 — Output signal vs strength of externally applied axial magnetic field.
(Response of pyroelectric detector = 1.5×10^4 watts/volt.)

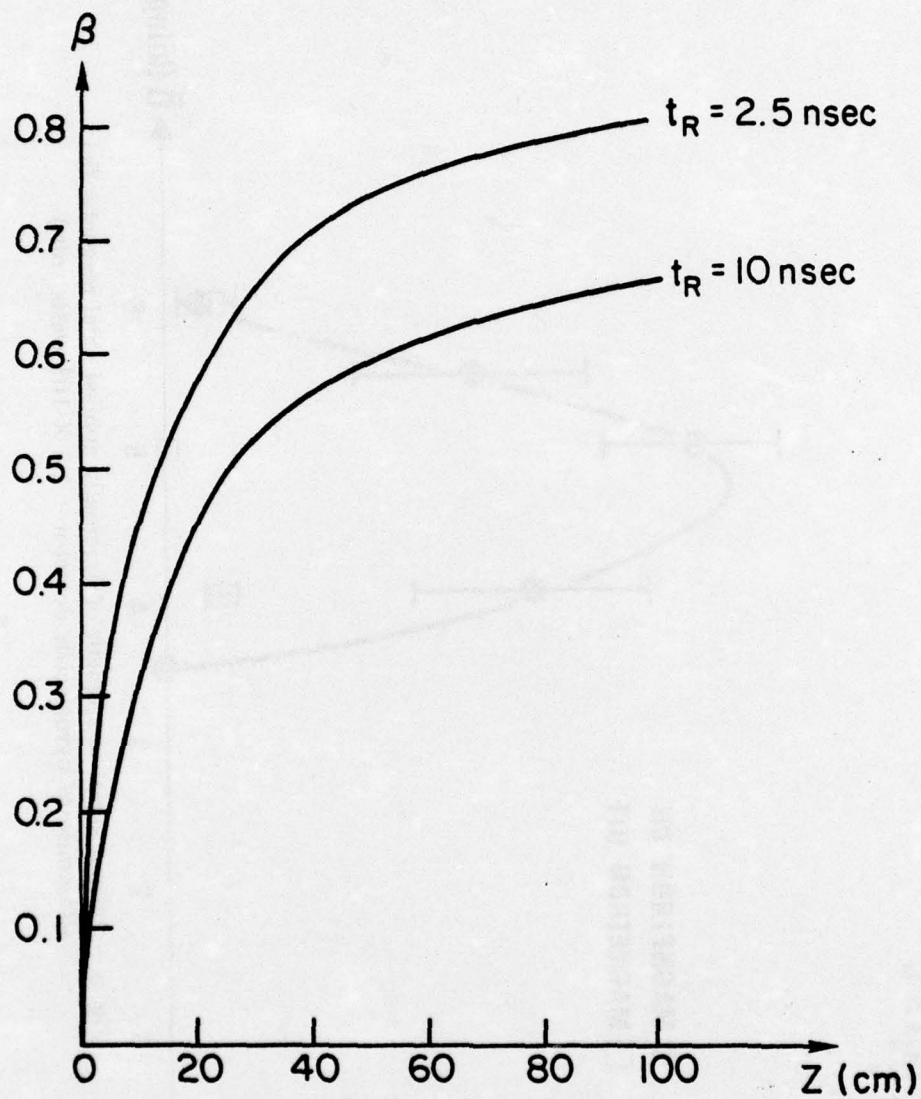


Fig. 9 — Velocity of the leading electrons
vs axial position of the beam front

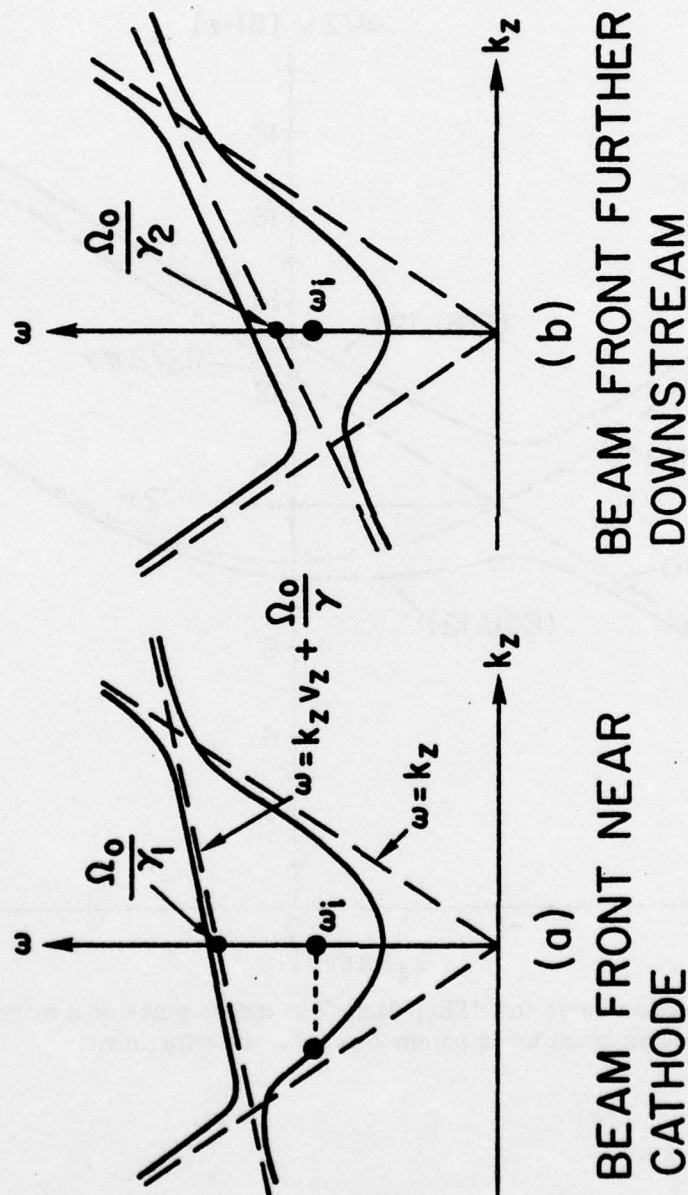


Fig. 10 — Dispersion curves for the "TE₁₁ Mode" in the presence of a magnetized electron beams showing that beam front scattering may occur only in certain portions of the drift tube

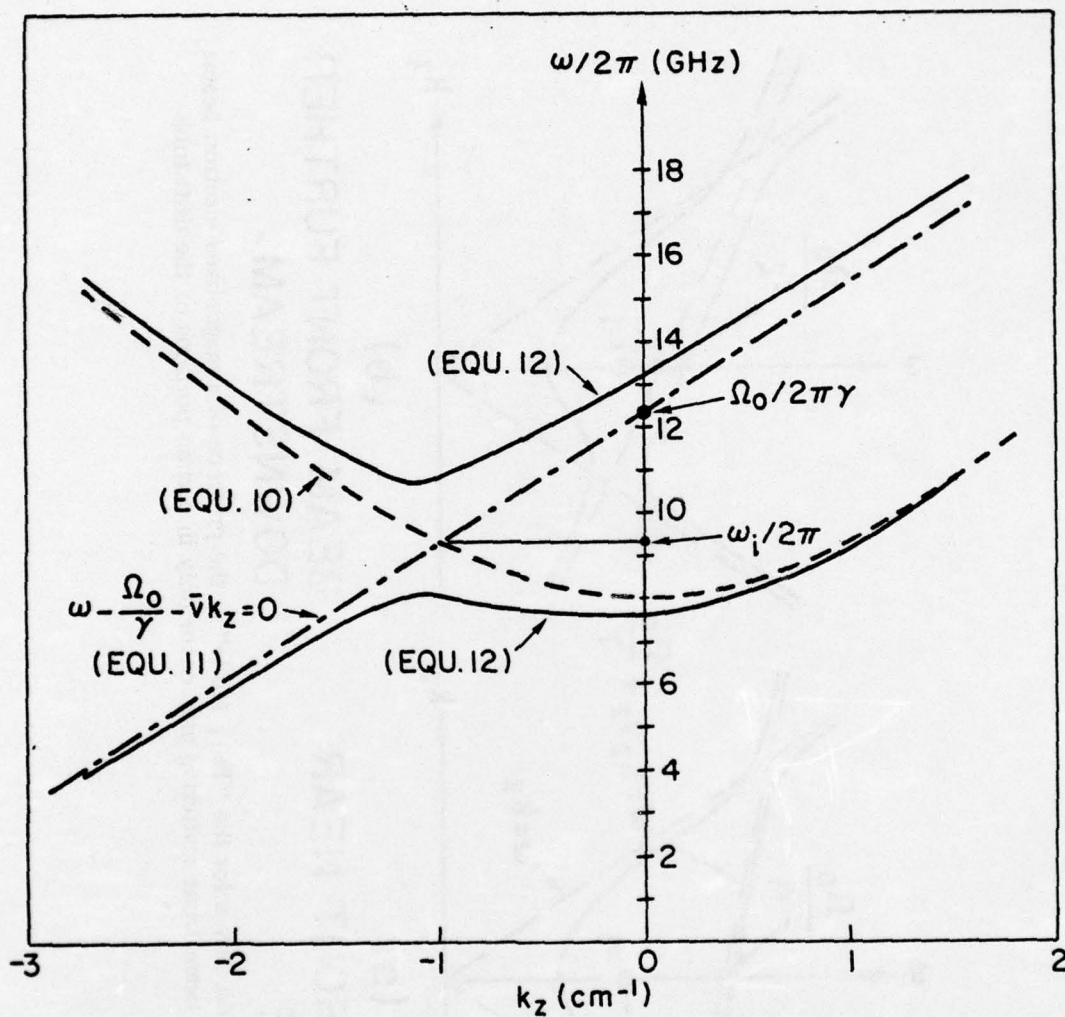


Fig. 11 — Dispersion curve for "TE₁₁ Mode" in the presence of a magnetized electron beam using parameters from the experiment

APPENDIX

The exact theory for the partially filled waveguide shown in Fig. 1 is straightforward, but it yields a very complicated transcendental dispersion relation.¹² To compute the dispersion relation required for this paper, we have therefore developed an approximate approach based upon the assumption that the true fields differ only slightly from the empty waveguide fields. This technique yields an algebraic dispersion relation which is readily solved. The special case of a completely filled guide has been treated exactly by Bevc and Everhart,¹³ and our results are found to agree well with theirs for densities such that $\omega_p \leq \frac{1}{4} \omega_o$, where ω_p and ω_o are respectively the frame invariant plasma frequency and the incident wave frequency in the beam frame.

We begin our analysis in the beam frame. Assuming that the fields vary as $\exp [i(k_o z + \ell \theta - \omega_o t)]$, the linearized wave equations for E_z and B_z are

$$\left\{ \begin{array}{l} \nabla^2 E_z + \frac{\omega_o^2}{c^2} E_z = -i\mu\omega_o \delta J_z - ik_o e \delta n / \epsilon \end{array} \right. , \quad (A1)$$

$$\left\{ \begin{array}{l} \nabla^2 B_z + \frac{\omega_o^2}{c^2} B_z = -\mu(\nabla \times \delta \tilde{J})_z \end{array} \right. , \quad (A2)$$

where μ and ϵ are respectively the permeability and permittivity of free space, E_z and B_z are the axial wave fields, and $\delta \tilde{J}$ and δn are respectively the first order current density and number density which drive the fields and which satisfy the continuity equation $-\frac{\partial}{\partial t} (e \delta n) + \nabla \cdot \delta \tilde{J} = 0$. We also

have $\delta \tilde{J} = -en_0 \delta v S(r - r_b)$, where n_0 is the zero order number density in the beam frame, $S(r - r_b)$ is the step function and the first order velocity δv is found from the equation of motion.

The fields expressed as an expansion of the empty waveguide fields are

$$E_z = \sum_n A_n J_\ell(a_{\ell n} r) e^{i(k_0 z + \ell \theta - \omega_0 t)}; \quad J_\ell(a_{\ell n} r_g) = 0,$$

$$B_z = \sum_n B_n J_\ell(b_{\ell n} r) e^{i(k_0 z + \ell \theta - \omega_0 t)}; \quad J'_\ell(b_{\ell n} r_g) = 0,$$

where J_ℓ is the Bessel function of order ℓ . The transverse fields are expressed in terms of the longitudinal fields in the usual way, but now we must include both TE and TM contributions since there are no pure modes for the partially filled magnetized waveguide.

Substituting the expressions for the expanded fields and the appropriate source terms into the wave equations and operating on Eq. (A1) with $\int_0^r g dr J_\ell(a_{\ell m} r)$ and on Eq. (A2) with $\int_0^r g dr J_\ell(b_{\ell m} r)$, one obtains

$$A_m \left(\frac{\omega_0^2}{c^2} - k_0^2 - a_{\ell m}^2 \right) \left(\frac{\omega_0^2 - \Omega_0^2}{\omega_p^2} \right) \\ = \sum_n A_n P_{\ell mn} + \frac{ia_{\ell m}}{T_\ell(a_{\ell m})\omega_0} \sum_n B_n \frac{\sqrt{b_{\ell n}^2 + k_0^2}}{b_{\ell n}} Z_{\ell mn}, \quad (A3)$$

$$B_m \left(\frac{\epsilon_0^2}{c^2} - k_o^2 - b_{lm}^2 \right) \left(\frac{\omega_o^2 - \Omega_o^2}{\omega_p^2} \right) \\ = \sum_n B_n Q_{lmn} - \frac{ib_{lm}}{cT_\ell(b_{lm})} \sum_n A_n \frac{1}{a_{ln}} Z_{lnm}, \quad (A4)$$

where

$$\omega_p^2 = \frac{e^2 n_o}{\epsilon m_o}.$$

$$P_{lmn} = \frac{1}{T_\ell(a_{lm})} \left\{ \frac{\omega_o^2 - \Omega_o^2}{\omega_o^2} \left(\frac{\omega_o^2}{c^2} - k_o^2 \right) \eta^2 U_\ell(a_{ln}, a_{lm}) \right. \\ \left. + \frac{a_{lm}}{a_{ln}} k_o^2 \eta^2 U_{\ell-1}(a_{ln}, a_{lm}) - \ell k_o^2 \left(1 - \frac{\Omega_o}{\omega_o} \right) \frac{1}{a_{ln}^2 r_g^2} J_\ell(a_{ln} r_b) J_\ell(a_{lm} r_b) \right\},$$

$$Q_{lmn} = \frac{\sqrt{b_{ln}^2 + k_o^2}}{T_\ell(b_{lm})} \left\{ \frac{\omega_o}{c} \frac{b_{lm}}{b_{ln}} \eta^2 U_{\ell-1}(b_{ln}, b_{lm}) \right. \\ \left. - \ell \frac{\omega_o}{c} \left(1 - \frac{\Omega_o}{\omega_o} \right) \frac{1}{b_{ln}^2 r_g^2} J_\ell(b_{ln} r_b) J_\ell(b_{lm} r_b) \right\},$$

$$Z_{lmn} = k_o \Omega_o \eta^2 U_{\ell-1}(a_{lm}, b_{ln}) + \ell k_o \left(1 - \frac{\Omega_o}{\omega_o} \right) \frac{\omega_o}{a_{lm} b_{ln} r_g^2} J_\ell(a_{lm} r_b) J_\ell(b_{ln} r_b),$$

$$\eta = \frac{r_b}{r_g},$$

$$T_{\ell}(a) = \frac{1}{r_g^2} \int_0^{r_g} J_{\ell}^2(ar) r dr ,$$

$$U_{\ell}(a, b) = \frac{1}{r_b^2} \int_0^{r_b} J_{\ell}(ar) J_{\ell}(br) r dr .$$

Equation (A3) is the dispersion relation for a $TM_{\ell m}$ mode that is modified by the presence of magnetized electrons so that it is no longer purely transverse magnetic. Similarly, Eq. (A4) represents the modified $TE_{\ell m}$ mode.

At this point the assumption is made that the $n = m$ term of each sum dominates. This assumption is plausible for low electron density where there should be little coupling between modes. Putting $n = m$ in Eqs. (A3) and (A4) and combining the two gives the total dispersion relation for the system:

$$\left[\left(\frac{\omega_o^2}{c^2} - k_o^2 - a_{\ell m}^2 \right) \frac{\omega_o^2 - \Omega_o^2}{\omega_p^2} - P_{\ell m m} \right] \left[\left(\frac{\omega_o^2}{c^2} - k_o^2 - b_{\ell m}^2 \right) \frac{\omega_o^2 - \Omega_o^2}{\omega_p^2} - Q_{\ell m m} \right] \\ = \frac{1}{T_{\ell}(a_{\ell m}) T_{\ell}(b_{\ell m})} \frac{\sqrt{b_{\ell m}^2 + k_o^2}}{\omega_o c} Z_{\ell m m}^2 . \quad (A5)$$

Now if we want the dispersion relation for the modified $TE_{\ell m}$ mode, we replace ω_o by the empty waveguide value $\omega_o = c(k_o^2 + b_{\ell m}^2)^{1/2}$ in the source terms (those corresponding to the right hand side of Eq. (A4)). Then we obtain

$$\left(\frac{\omega_o^2}{c^2} - k_o^2 - b_{lm}^2 \right) (\omega_o^2 - \Omega_o^2) = \frac{\frac{\omega_p^2}{c^2}}{T_\ell(a_{lm})T_\ell(b_{lm})} \frac{Z_{lm}^2}{\left(b_{lm}^2 - a_{lm}^2 \right) \left(\frac{\omega_o^2 - \Omega_o^2}{\omega_p^2} \right) + P_{lm}} - Q_{lm} \frac{\omega_p^2}{c^2} . \quad (A6)$$

Equation (A6) is the desired dispersion relation in the beam frame. It is a simple matter to Lorentz transform to the laboratory frame. Letting k_z and ω denote quantities in the laboratory frame the Lorentz transformations are:

$$k_o = \gamma \left(k_z - \beta \frac{\omega}{c} \right) ,$$

and

$$\omega_o = \gamma (\omega - \beta k_z c) .$$

REFERENCES

1. R. H. Pantell, G. Soncini, and H. E. Puthoff, IEEE J. Quantum Electron. QE-4, 905 (1968).
2. V. P. Sukhatme and P. E. Wolf, J. Appl. Phys. 44, 2331 (1973); IEEE J. Quantum Electron. QE-10, 870 (1974).
3. P. Sprangle and V. L. Granatstein, Appl. Phys. Lett. 25, 377 (1974); and, P. Sprangle, V. L. Granatstein, and L. Baker, Phys. Rev. A 12, 1697 (1975).
4. J. M. J. Madey, J. Appl. Phys. 42, 1906 (1971).
5. C. Max and F. W. Perkins, Phys. Rev. Lett. 27, 1342 (1971).
6. V. L. Granatstein, M. Herndon, R. K. Parker, and S. P. Schlesinger, IEEE Trans. Microwave Theory Tech. MTT-22, 1000 (1974).
7. L. Elias, W. Fairbank, J. M. J. Madey, H. A. Schwettman, and T. Smith, Phys. Rev. Lett. 36, 717 (1976).
8. K. Landecker, Phys. Rev. 86, 852 (1952).
9. R. K. Parker and M. Ury, IEEE Trans. Nuclear Sci. NS-22, 983 (1975).
10. M. Friedman and M. Ury, Rev. Sci. Instrum. 41, 1334 (1970).

11. R. E. Collin, Foundations of Microwave Engineering (McGraw-Hill, New York 1966), p. 340.
12. W. P. Allis, S. J. Buchsbaum, and A. Bers, "Waves in Anisotropic Plasmas" (M.I.T. Press, Cambridge, Mass. 1963) p. 239.
13. V. Bevc and T. E. Everhart, J. Electronics and Control 13, 185 (1962).